Published in final edited form as:
Comput Med Imaging Graph. 2014 July ; 38(5): 403–410. doi:10.1016/j.compmedimag.2014.03.007.

Fuzzy logic color detection: Blue areas in melanoma dermoscopy images

Mounika Lingala[a,1], **R. Joe Stanley**[b,2], **Ryan K. Rader**[c,3], **Jason Hagerty**[c,3], **Harold S. Rabinovitz**[d,4], **Margaret Oliviero**[d,4], **Iqra Choudhry**[c,3], and **William V. Stoecker**[c,*]

[a] Department of Electrical and Computer Engineering, Missouri University of Science and Technology, G20 Emerson Electric Company Hall, 301 West 16th Street, Rolla, MO 65409-0040, United States

[b] Department of Electrical and Computer Engineering, Missouri University of Science and Technology, 127 Emerson Electric Company Hall, 301 West 16th Street, Rolla, MO 65409-0040, United States

[c] Stoecker & Associates, LLC 10101 Stoltz Drive Rolla, MO 65401-7714, United States

[d] Skin & Cancer Associates, 201 NW 82nd Avenue, Suite 501, Plantation, FL 33324, United States

Abstract

Fuzzy logic image analysis techniques were used to analyze three shades of blue (lavender blue, light blue, and dark blue) in dermoscopic images for melanoma detection. A logistic regression model provided up to 82.7% accuracy for melanoma discrimination for 866 images. With a support vector machines (SVM) classifier, lower accuracy was obtained for individual shades (79.9–80.1%) compared with up to 81.4% accuracy with multiple shades. All fuzzy blue logic alpha cuts scored higher than the crisp case. Fuzzy logic techniques applied to multiple shades of blue can assist in melanoma detection. These vector-based fuzzy logic techniques can be extended to other image analysis problems involving multiple colors or color shades.

Keywords

Fuzzy logic; Dermoscopy; Blue area; Image analysis; Melanoma; Dysplastic nevi

* Corresponding author. wvs@mst.edu (W.V. Stoecker)..
ml427@mst.edu (M. Lingala), stanleyj@mst.edu (R. Joe Stanley), rkrc5b@health.missouri.edu (R.K. Rader), hagerty.jason@gmail.com (J. Hagerty), harold@admcorp.com (H.S. Rabinovitz), maggie@admcorp.com (M. Oliviero), iqrachowder@live.com (I. Choudhry)
[1]Tel.: +1 573 341 4518; fax: +1 573 341 4532.
[2]Tel.: +1 573 341 6896; fax: +1 573 341 4532.
[3]Tel.: +1 573 364 0122; fax: +1 573 364 0129.
[4]Tel.: +1 954 473 6750; fax: +1 954 424 7093.

Conflicts of interest statement
The authors declare they do not hold any conflicts of interest that could inappropriately influence this manuscript.

1. Introduction

Of all skin cancers, invasive malignant melanoma exacts the highest total mortality with an estimated incidence of 76,250 and an estimated total of 9180 deaths in the United States in 2012 alone [1]. The incidence rate for melanoma has risen tenfold over the past 60 years [2]. Earlier detection of melanoma is crucial, as diagnosis at the earliest *in situ* stage does not alter life expectancy [3]. Dermoscopy is a non-invasive imaging technique that employs magnification in combination with reduction of skin surface reflections. Dermoscopy improves sensitivity, specificity and accuracy in melanoma detection [4–7], by enhancing visualization of many features, including shades of blue [7–10].

Blue coloration is present within several dermoscopic features: homogeneous blue pigmentation; blue-white veil, and blue-black color. Homogeneous blue pigmentation is a first-step criterion in the 2-step procedure for examining pigmented skin lesions [8]. Blue-white veils are defined as irregular structureless areas of confluent blue pigmentation with an overlying white “ground-glass” appearance [9]. These structures allow semi-automatic discrimination of melanoma from benign lesions with an accuracy of 82.9% on a more advanced lesion set with blue that is easier to detect [10]. In clinical studies, a blue color is one of the positive criteria within the 7-point checklist for suspicious melanocytic skin lesions [8] and a blue-black color rule has been suggested as an indicator of pigmented nodular melanoma [11]. We analyzed 195 melanoma images and noted 22 with prominent blue pigmentation. In contrast to earlier studies [9,10], few lesions within the image set presented in the clinic with fully developed blue veils or blue-black areas. We therefore focused on shades of blue found in melanomas now seen in clinics at an early stage, often at the pre-invasive (*in situ*) stage [12–14].

Three shades of blue were chosen for analysis: light blue, dark blue, and lavender blue (Fig. 1). Melanoma classification has been previously studied using color-derived features [15–18]. We are not aware of any previous analysis of specific color shades in a machine learning approach for melanoma discrimination.

There have been numerous studies exploring fuzzy logic techniques for color analysis and segmentation in medical applications. Some of the fuzzy logic methods investigated in previous research for color and skin analysis include color histogram analysis for color labeling and skin lesion discrimination [19], blotch size estimation for skin lesion discrimination [20], blotch detection in skin lesions using fuzzy clustering and texture segmentation [21], fuzzy clustering for adaptively removing background skin color for skin color region segmentation [22], fuzzy c-means clustering for skin lesion segmentation [23], adaptive fuzzy c-means using local spatial continuity for cluster prototype estimation [24], and skin region segmentation using fuzzy decision tree modeling [25].

In this article, we present a fuzzy set representation to segment blue areas in melanoma images for discrimination from benign lesions using red, green, and blue chromaticity, relative RGB color, value (from the HSV color space) and the blue:green ratio. The order of the remaining sections of the article is as follows: Section 2 describes the image set, absolute thresholding procedure, fuzzy set characterization, blue shade segmentation, feature

extraction techniques and classification method; Section 3 provides the results; Section 4 pertains to the discussion; Section 5 elaborates on potential future work in blue area segmentation and Section 6 presents conclusions.

2. Methods

Fig. 2 provides an overview of the experimental workflow including supervised blue shade segmentation and lesion discrimination using a training set to determine the membership function parameters. Detection of blue area was performed in two stages using the training set in the former stage and the test set in the latter: (1) manual blue area marking, determination of absolute threshold parameters, and fuzzy set implementation; and (2) automatic blue area mask generation, feature extraction, and classification.

2.1. Description of experimental data set

A test dataset of 866 contact, non-polarized dermoscopic images (173 melanoma and 693 benign acquired dysplastic and congenital nevi) were acquired in the course of the study NIH CA101639-02A2. All melanomas were verified by histopathological examination by a dermatopathologist. All benign lesions were evaluated with dermoscopy. All lesions with any concern by either patient or physician were either biopsied or were followed in the clinic and found to be reliably benign. For fuzzy set development for the different blue area color shades, a training set of 22 additional melanoma images with blue areas was examined. In total, there were 888 images, with 195 melanomas in the training and test set. Of the melanomas, 110 were at the *in situ* stage and 85 were at the invasive stage, giving a ratio of *in situ* to invasive malignant melanomas = MIS:MM = 1.29. All images had 1024 × 768 resolution and were contact non-polarized dermoscopy images acquired using 3Gen DermLite Fluid Dermatoscope (3Gen Inc., Dana Point, CA) with a Sony DSC-W70 7.2 megapixel digital camera and a dermoscopic adapter. This research was approved by Phelps County Regional Medical Center Institutional Review Board, Rolla, MO, USA, according to the Helsinki Declaration. Informed consent was obtained from all participants.

2.2. Manual blue area marking

Three small, uniform-sized elliptical areas in each of the 22 training image melanomas with blue areas were manually selected for analysis in each lesion with the guidance of a dermatologist (W.V.S.) using a second-order best-fit B-spline to connect the border points manually selected by the dermatologist to create a closed border curve [26]. An example of these selections is shown in Fig. 3. Since melanoma images could have any shade or shades of blue, and it was not known a priori how to precisely define which shades were present, the widest possible range of blue shading was marked. These areas were then classified as light blue, dark blue, or lavender blue and used for pre-processing and threshold determination, following the training process for color parameter determination and blue area segmentation and analysis steps in Fig. 2.

2.3. Feature characterization – pre-processing and absolute thresholding

To equalize the color changes due to different skin types and processing techniques, the relative color approach was used. For this approach, the average RGB color of each pixel

inside the lesion was calculated by subtracting the average RGB color of the surrounding skin, using methods previously described [15–18]. The surrounding skin region was an area equal to 20% of the lesion area encircling the border plus an additional 10-pixel wide margin. The relative RGB color values were used for subsequent analysis.

Upper and lower absolute color threshold ranges were empirically determined from a training set of 22 melanoma images for the chromaticity of each color within the RGB color model using ChrX = X/(R + G + B); X ∈ {R, G, B}. The three chromaticity components for a pixel are: ChrR, ChrG, and ChrB; the optimized chromaticity thresholds are represented by $ChrR_{opt}$, $ChrG_{opt}$, and $ChrB_{opt}$. These optimized thresholds were within bounds based on observations from a dermatologist (W.V.S.) on the manually marked areas. Pixels must satisfy these chromaticity thresholds: (1) $ChrR_{opt1} < ChrR < ChrR_{opt2}$, (2) $ChrG_{opt1} < ChrG < ChrG_{opt2}$, (3) $ChrB_{opt1} < ChrB < ChrB_{opt2}$, where the lower and upper bounds opt1 and opt2, respectively, were determined empirically from the melanoma training set of lesions. Fig. 4b is an example of a blue area mask generated using the chromaticity thresholds from the original image, Fig. 4a.

Lavender blue was easily separated from the other two shades of blue (light blue and dark blue) using chromaticity thresholds determined empirically on the 22-image training set. Separating the other two shades of blue, which differ in brightness, was best accomplished using intensity (*V*) alone. An empirically optimized brightness threshold was calculated as: $V_{opt} = 0.5V_m + 0.224$, where 0.224 represents the median brightness value and V_m is the median brightness for all light and dark blue areas computed from the 22-image melanoma training set. Finally, falsely detected blue areas were removed by requiring that candidate pixels satisfy the inequality: $B/G > B/Gopt$, where *B/Gopt* is the optimized blue:green color ratio empirically determined as 0.92 from the training set.

2.4. Construction of fuzzy sets

To determine the color parameters for the blue area membership functions, we examined fuzzy set representations to define the parameters of each color shade by extending previous research using fuzzy sets to characterize color in skin lesion histograms [19] and blotches in dermoscopy skin lesion images [20]. In this research, a fuzzy set is specified to provide high membership to pixels within the skin lesion image that perceptually contribute to identifying blue areas. The advantage of fuzzy sets is that they provide degrees of membership that can be representative of lighter or darker blue areas. This is beneficial from a dermatologic perspective because it allows for inter-shade variation and color variation between lesion images.

For red and blue chromaticity thresholds, trapezoidal membership functions were used such that a membership value of 1 could be designated for all values between the absolute upper and lower thresholds and a lesser degree of membership to the ramp on both sides of absolute thresholds. Z-shaped and S-shaped membership functions were given to green chromaticity and relative colors, respectively, as they each had a single absolute threshold value. A membership value of 1 was designated to all the values specified by the single threshold and a degree of membership was denoted to those within the ramp of the membership function.

The membership function for red chromaticity $\mu_{\text{red-chrom}}(x)$ which depends on four parameters is given in Eq. (1).

$$\mu_{\text{red\_ chrom}}(x) = \left\{ \begin{array}{c} 0, x \leq a \\ \frac{x-a}{b-a}, a \leq x \leq b \\ 1, b \leq x \leq c \\ \frac{d-x}{d-c}, c \leq x \leq d \\ 0, d \leq x \end{array} \right\} \quad (1)$$

Let *RX* be the set of red chromaticity values for three different shades with $X \in$ {light blue, dark blue and lavender blue}. The red chromaticity set R_lightblue ranges from 0.21 to 0.4, R_darkblue also ranges between 0.21 and 0.4 and R_lavenderblue ranges from 0.33 to 0.5. The fuzzy set is the pair (*RX*, $\mu_{\text{red\_chrom}}(x)$) where $\mu_{\text{red\_chrom}}$:$RX \rightarrow$ [0,1]. All the values in the sets *RX* have a degree of membership.

Four parameters, *a*, *b*, *c* and *d*, of the trapezoidal functions, determine the degree of membership. All the values between the parameters *b* and *c* were fully included in the fuzzy set as $\mu_{\text{red\_chrom}}(x) = 1$ and any value less than *a* or greater than *d* were designated as red chrom(x) = 0. Values between a and b have a membership value dependent on the alpha cuts; similarly, the membership values between *c* and *d* were also dependent on alpha cuts.

Fuzzy sets were also constructed based on trapezoidal membership function for blue chromaticity thresholds of lavender blue and combined light and dark blue. This membership function for blue chromaticity is $\mu_{\text{red\_chrom}}(x)$ defined in Eq. (2).

$$\mu_{\text{blue\_ chrom}}(x) = \left\{ \begin{array}{c} 0, x \leq a \\ \frac{x-a}{b-a}, a \leq x \leq b \\ 1, b \leq x \leq c \\ \frac{d-x}{d-c}, c \leq x \leq d \\ 0, d \leq x \end{array} \right\} \quad (2)$$

The fuzzy sets for blue chromaticity can be denoted with the pair (*BX*, $\mu_{\text{blue\_chrom}}$), where $\mu_{\text{blue\_chrom}}$:$BX \rightarrow$ [0,1] and *BX* are the sets for blue chromaticity values of different shades with $X \in$ {light blue, dark blue and lavender blue . Blue chromaticity set values range from 0.24 to 0.49 for light blue and dark blue and 0.24–0.42 for lavender blue. Four parameters of the trapezoidal membership functions for blue chromaticity of different shades are listed in Table 1.

Fuzzy set pair (*GX*, $\mu_{\text{green\_chrom}}$) with $\mu_{\text{green\_chrom}}$:$GX \rightarrow$ [0,1] and *GX* being the green chromaticity set ranging from 0 to 0.38 for lavender blue was defined for green chromaticity. Z-shaped membership function denoted as $\mu_{\text{green\_chrom}}(x)$ was based on two parameters and defined in Eq. (3).

$$\mu_{\text{green\_ chrom}}(x) = \left\{ \begin{array}{c} 1, x \leq a \\ 1 - 2\left(\frac{x-a}{b-a}\right)^2, a \leq x \leq \frac{a+b}{2} \\ 2\left(\frac{x-b}{b-1}\right)^2, \frac{a+b}{2} \leq x \leq b \\ 0, x \geq b \end{array} \right\} \quad (3)$$

where *a* locates the left extreme of the sloped portion of the curve and *b* locates the right extreme of the curve.

The final fuzzy sets for relative color are defined using S-shaped membership functions. Let RelativeX denote the set with all possible relative color values ranging from −255 to 255, then the fuzzy set is the pair (RelativeX, μ_{red_chrom}) where μ_{red_chrom}:Relative X → [0,1]. The S-shaped membership function μ_{red_chrom} is given in Eq. (4).

$$\mu_{\text{rel\_ chrom}}(x) = \left\{ \begin{array}{c} 1, x \leq a \\ 1 - 2\left(\frac{x-a}{b-a}\right)^2, a \leq x \leq \frac{a+b}{2} \\ 2\left(\frac{x-b}{b-1}\right)^2, \frac{a+b}{2} \leq x \leq b \\ 0, x \geq b \end{array} \right\} \quad (4)$$

where *a* and *b* define the left and right extremes of the sloped portion of the curve. For light blue, dark blue and lavender blue, all the relative color values above b are fully included in the fuzzy set and values below a are not included in the fuzzy set. Values between a and b have membership values depending on the alpha cut. Table 1, columns 3–6, shows the parameters used for different fuzzy sets to segment the blue areas.

2.5. Blue shades segmentation

Three shades of blue were segmented with various combinations of fuzzy sets. The fuzzy sets for red chromaticity, blue chromaticity and relative color were the same for light and dark blue shades. The weighted brightness threshold V_{opt} was placed on these combined areas to separate light blue and dark blue. Light and dark blue areas were separately segmented based on applying alpha cuts, *e.g.* specified membership values, for different combinations of color fuzzy sets, whereby, a pixel is included in the segmented light or dark blue area mask if the pixel satisfies the alpha-cut membership constraints for the specified combination of color fuzzy sets. Lavender blue was segmented using the red chromaticity, blue chromaticity, green chromaticity, and relative color fuzzy sets. Results of blue area segmentation are shown (Fig. 5).

2.6. Feature extraction

Different alpha-cut combinations were investigated to generate segmented blue area regions for feature and lesion discrimination analysis. Various contour features, color features and texture features listed in the following section were extracted for the analysis. A total of 150 features were derived, using each of the 3 color shades.

2.6.1. Contour features

- Eccentricity of the largest blob (*E*): $E=D/\sqrt{A}$; Returns the eccentricity value by calculating the Euclidean distance (*D*) between the centroid of largest blob and the centroid of the lesion, then dividing it with square root of the lesion area (*A*)
- Relative size of all blobs (*R*): $R=\sum_{i=1}^{n} B_i/A$; measures the relative by size dividing the sum of all blob areas (B_i) by the area of the lesion (*A*); *n* is the number of blobs in the lesion

- Relative size of largest blob (*S*): $S = B_{max}/A$; ratio of the largest blob area (B_{max}) within the lesion and area of the lesion (*A*)
- Absolute size of largest blob: area of largest blob within the lesion
- Number of blobs in the lesion.

2.6.2. Color features

- Blue areas by quintiles: measures the blue areas present within each lesion quintile created by the Euclidean distance transform. The outer 5th of all pixels closest to the lesion boundary are the 1st quintile, and the inner 5th of all pixels are closest to the center, modified from [27].
- Average RGB values
- Maximum and minimum values
- Standard deviation: measures the variation of RGB values in blue areas
- Chromaticity: ChrX = $X/(R + G + B)$; $X \in \{R, G, B\}$

2.6.3. Texture features

- Mean (μ): $\mu = \sum_{l=0}^{L-1} r_i p(r_i)$; measured for grayscale and RGB planes.
- Here, r_i is a variable indicating the gray level of RGB value and $p(r_i)$ is the probability of the occurrence of r_i. *L* is the number of possible gray levels.
- Variance (δ^2): $\sigma^2 = \sum_{l=0}^{L-1} (r_i - \mu)^2 p(r_i)$; measures the average contrast of blue areas in all the three RGB planes, as well as in grayscale.
- Smoothness (*S*): $S = 1 - (1/(1 + \delta^2))$; measures the smoothness of blue areas; its value is near zero for very smooth areas and near one for unsmooth regions.
- Skewness (*k*): $\kappa = \sum_{l=0}^{L-1} (r_i - \mu)^3 p(r_i)$; gives the skewness of blue area histograms. It returns a value of zero for symmetric histograms about the mean; a positive value for right skewed histograms; and a negative value for left skewed histograms.
- Uniformity (U): $U^U = \sum_{l=0}^{L-1} p^2(r_i)$; returns a maximum value when all gray levels or red, green and blue values are equal in all the blue areas.
- Entropy (*e*): $e = -\sum_{l=0}^{L-1} p(r_i) \log_2 p(r_i)$; measures the randomness or uncertainty of values over blue areas.

2.7. Classification

A ten-fold cross-validation approach was used to generate training and testing sets using 173 melanomas and 693 benign lesions. The features for each training/test set were normalized based on subtracting the mean and dividing by the standard deviation feature values as

determined from the training set. Fan's implementation of a support vector machine (SVM) was utilized for skin lesion classification [28,29]. The SVM algorithm used a linear kernel [28] and parameter settings based on the implementation in [29]. Classification results were obtained for different alpha cuts for all the three shades of blue.

3. Results

The blue shade segmentation algorithm in II.E was applied to a test set of 866 dermoscopic skin lesion images, including 173 melanoma and 693 benign lesions, using different alpha cuts to the red chromaticity, blue chromaticity, green chromaticity, and relative color fuzzy sets to generate blue area masks. Alpha cuts ranging from 0.25 to 0.75 were observed in increments of 0.05; the alpha cut of 1 represents the absolute threshold, *i.e*. the non-fuzzy case, also termed the crisp case. Melanoma and benign lesion discrimination was performed by using the SVM classifier on the features extracted from final color masks for light blue, dark blue, and lavender blue at the varied alpha cuts. Table 2 lists the diagnostic results obtained for different alpha cuts using a support vector machine (SVM) classifier.

The accuracy for individual shades ranged from 79.9% to 80.1%, with the highest accuracy (81.4%) obtained at an alpha cut of 0.25 using the SVM classifier for all three shades. Fig. 6 shows an example of different alpha cuts to determine lavender blue areas. As the alpha cut value is decremented, the restrictiveness on the threshold relaxes, resulting in a larger area determination.

The features obtained from the final masks of all three blue shades were combined for comprehensive analysis of blue areas. Diagnostic accuracy was measured at different alpha cuts for the combined features. In addition to the SVM classifier, the logit logistic regression model of Statistical Analysis Software (SAS Corp., Cary, NC) was used for analysis. The alpha cut of 0.35 gave the highest accuracy of 82.7% using logit analysis. Discrimination maximum accuracy using the final logistic regression model for all three shades was similar (within 1.5%) to results for SVM at all alpha cuts (Table 3).

We examined the receiver operating characteristic (ROC) curves based on the logit logistic regression model using SAS which plots the sensitivity *versus* one minus specificity. The combined ROC curves (Fig. 7) depict the results of area under the ROC curve (AUC) of different alpha cuts ranging from 0.25 to 0.65 with 0.1 increments.

Statistical analysis of variables was performed the same logistic regression model for the test set of 866 images. Table 4 shows statistics for the eight most significant variables present in the final model for the alpha cut = 0.65 which attained the highest accuracy, 82.7%.

4. Discussion

This study analyzes the implementation of fuzzy set techniques on blue area segmentation for melanoma discrimination from benign lesions. Accuracy of up to 82.7% was obtained at alpha cuts of 0.3, 0.4, and 0.65 from the features derived on the 866-image test set using logistic regression. The diagnostic accuracy was improved for the combined shades over the accuracy of individual shades. Fuzzy logic allowed optimization over alpha cuts, with all

alpha cuts showing higher AUC than the crisp case (AUC 68.8% for alpha = 1.0). To our knowledge, this work is the first to exploit the presence of multiple critical shades of a color to enable automatic detection of early melanoma and the first to employ fuzzy logic to detect those color shades.

There are clinical correlates for the three most important features found by logistic regression. Blue itself corresponds to the Tyndall effect, the optical phenomenon of preferential reflection of short wavelengths from melanin present deep within the lesion. Lavender blue is newly described here. We hypothesize that lavender blue represents erythema coinciding with blue, giving a red tinge to the blue area. The erythema represents physiologic expansion of blood vessels, shown by subsurface transillumination to be a marker for skin cancer [30]. The most important features retained in logistic regression (Table 4) are derived from lavender blue areas, corresponding to this combination of blue from deep melanin and red from the blood vessels.

This study extends an observation made by Menzies and colleagues [31]: multiple shades of pink were associated with amelanotic melanoma. Here we extend this research to the detection of multiple blue shades using automatic segmentation by fuzzy logic.

The empirical nature of the observed color shade definitions represents a drawback in this study. This is an ‘anthroporphic’ modeling of color representation, that is,color plane cuts for the different shades are determined to match the shades observed by the dermatologist. This method, although entailing the drawbacks of empirical diagnostic modeling, can help elucidate the diagnostic process. The fuzzy logic process, using alpha cuts as shown in this study, allows data-driven optimization of the empirically determined color plane thresholds.

5. Conclusions

In this article, blue areas present in dermoscopic images of skin lesions were used to discriminate melanoma from benign lesions by fuzzy logic implementation. The method segments three shades of blue using a combination of alpha-cut membership functions, and characterizes and classified images based on key color parameters. A logistic regression model provided up to 82.7% accuracy for melanoma discrimination for 866 images. With a support vector machines (SVM) classifier, lower accuracy was obtained for individual shades (79.9–80.1%) compared with up to 81.4% accuracy with multiple shades.

6. Future work

For future work, additional features can be included to improve the accuracy and the corner points of the membership functions can be varied to further optimize melanoma discrimination.

Weaknesses in the current study include the relatively small set of lesions analyzed, which limit the power of conclusions drawn here. Future work includes the inclusion of more lesions in the analysis and the use of automatic borders in lesion analysis. Additionally, blood volume as a marker for malignancy was shown in the work of Terushkin et al. to be increased in more advanced malignancies [30]. One hypothesis that could be tested with

malignancies at various stages is that infrared illumination may play a greater role in detection of more advanced malignancies.

Acknowledgments

We appreciate the efforts of the dermatologists at Skin & Cancer Associates, LLC (Plantation, FL USA), Sheard & Drugge, PC (Stamford, CT USA), and The Dermatology Center (Rolla, MO USA) for their assistance in study recruitment and image acquisition.

Funding

This publication was made possible by Grant Number SBIR R44 CA-101639-02A2 of the National Institutes of Health (NIH).

Role of the sponsor

The contents of this article are solely the responsibility of the authors and do not necessarily represent the official views of NIH, the sponsor. The sponsor had no role in the design and conduct of the study; in the collection; analysis, and interpretation of data; or in the preparation, review, or approval of the manuscript.

References

1. Siegel R, Naishadham D, Jemal A. Cancer statistics, 2012. CA: Cancer J Clin. 2012; 62(1):10–29. [PubMed: 22237781]
2. SEER Cancer Statistics Review 1975-2009 (Vintage 2009 Populations). http://seer.cancer.gov/csr/1975.2009.pops09/index.html [Updated 30.04.12]
3. Mocellin S, Nitti D. Cutaneous melanoma in situ: translational evidence from a large population-based study. Oncologist. 2011; 16(6):896–903. [PubMed: 21632457]
4. Argenziano G, Puig S, Zalaudek I, Sera F, Corona R, Alsina M, et al. Dermoscopy improves accuracy of primary care physicians to triage lesions suggestive of skin cancer. J Clin Oncol. Apr; 2006 24(12):1877–82. [PubMed: 16622262]
5. Carli P, De Giorgi V, Chiarugi A, Nardini P, Weinstock MA, Crocetti E, et al. Addition of dermoscopy to conventional naked-eye examination in melanoma screening: a randomized study. J Am Acad Dermatol. May; 2004 50(5):683–9. [PubMed: 15097950]
6. Vestergaard ME, Macaskill P, Holt PE, Menzies SW. Dermoscopy compared with naked eye examination for the diagnosis of primary melanoma: a meta-analysis of studies performed in a clinical setting. Br J Dermatol. 2008; 159(3):669–76. [PubMed: 18616769]
7. Argenziano G, Soyer HP, Chimenti S, Talamini R, Corona R, Sera F, et al. Dermoscopy of pigmented skin lesions: results of a consensus meeting via the Internet. J Am Acad Dermatol. 2003; 48(5):679–93. [PubMed: 12734496]
8. Argenziano G, Fabbrocini G, Carli P, De Giorgi V, Sammarco E, Delfino M. Epiluminescence microscopy for the diagnosis of doubtful melanocytic skin lesions. Comparison of the ABCD rule of dermatoscopy and a new 7-point checklist based on pattern analysis. Arch Dermatol. 1998; 134(12):1563–70. [PubMed: 9875194]
9. Argenziano, G.; Soyer, HP.; De Giorgi, V.; Piccolo, D.; Carli, P.; Delfino, M., et al. Interactive atlas of dermoscopy. EDRA Medical Publishing & New Media; Milan, Italy: 2002.
10. Celebi ME, Iyatomi H, Stoecker WV, Moss RH, Rabinovitz HS, Argenziano G, et al. Automatic detection of blue-white veil and related structures in dermoscopy images. Comput Med Imaging Graph. 2008; 32(8):670–7. [PubMed: 18804955]
11. Argenziano G, Longo C, Cameron A, Cavicchini S, Gourhant JY, Lallas A, et al. Blue-black rule: a simple dermoscopic clue to recognize pigmented nodular melanoma. Br J Dermatol. 2011; 165(6):1251–5. [PubMed: 21916885]
12. Bassoli S, Borsari S, Ferrari C, Giusti F, Pellacani G, Ponti G, Seidenari S. Grey-blue regression in melanoma in situ-evaluation on 111 cases. J Skin Cancer. 2011:180980. [PubMed: 21748024]
13. Seidenari S, Bassoli S, Borsari S, Ferrari C, Giusti F, Ponti G, Tomasini C, Magnoni C. Variegated dermoscopy of in situ melanoma. Dermatology. 2012; 224(3):262–70. [PubMed: 22653091]

14. Seidenari S, Ferrari C, Borsari S, Benati E, Ponti G, Bassoli S, Giusti F, Schianchi S, Pellacani G. Reticular grey-blue areas of regression as a dermoscopic marker of melanoma in situ. Br J Dermatol. Aug; 2010 163(2):302–9. [PubMed: 20426776]
15. Cheng Y, Swamisai R, Umbaugh SE, Moss RH, Stoecker WV, Teegala S, et al. Skin lesion classification using relative color features. Skin Res Technol. 2008; 14(1):53–64. [PubMed: 18211602]
16. Stanley RJ, Stoecker WV, Moss RH. A relative color approach to color discrimination for malignant melanoma detection in dermoscopy images. Skin Res Technol. 2007; 13(1):62–72. [PubMed: 17250534]
17. Stanley RJ, Stoecker WV, Moss RH, Rabinovitz HS, Cognetta Jr AB, Argenziano G. A basis function feature-based approach for skin lesion discrimination in dermatology dermoscopy images. Skin Res Technol. 2008; 14(4):425–35. [PubMed: 18937777]
18. Stoecker WV, Wronkiewiecz M, Chowdhury R, Stanley RJ, Xu J, Bangert A, et al. Detection of granularity in dermoscopy images of malignant melanoma using color and texture features. Comput Med Imaging Graph. 2011; 35(2):144–7. [PubMed: 21036538]
19. Stanley RJ, Moss RH, Van Stoecker W, Aggarwal C. A fuzzy-based histogram analysis technique for skin lesion discrimination in dermatology clinical images. Comput Med Imaging Graph. 2003; 27(5):387–96. [PubMed: 12821032]
20. Khan A, Gupta K, Stanley RJ, Stoecker WV, Moss RH, Argenziano G, et al. Fuzzy logic techniques for blotch feature evaluation in dermoscopy images. Comput Med Imaging Graph. 2009; 33(1):50–7. [PubMed: 19027266]
21. Madasu VK, Lowell BC. Blotch detection in pigmented skin lesions using fuzzy co-clustering and texture segmentation. Proceedings of the Conference on Digital Image Computing: Techniques and Applications (DICTA'09). 2009:25–31.
22. Xiao K, Danghu L, Lansun S. Segmentation of skin color regions based on fuzzy cluster. Proceedings of the Symposium on Intelligent Multimedia, Video and Speech Processing. 2004:125–8.
23. Schmid P. Segmentation of digitized dermatoscopic images by two-dimensional color clustering. IEEE Trans Med Imag. 1999; 18(2):164–71.
24. Liew AW-C, Yan H, Law NF. Image segmentation based on adaptive cluster prototype estimation. IEEE Trans Fuzzy Sys. 2005; 13(4):444–53.
25. Bhatt RB, Sharma G, Dhall A, Chaudhury S. Efficient skin region segmentation using low complexity fuzzy decision tree model. Proceedings of the IEEE India Conference (INDICON). 2009:1–4.
26. Erkol B, Moss RH, Stanley RJ, Stoecker WV, Hvatum E. Automatic lesion boundary detection in dermoscopy images using gradient vector flow snakes. Skin Res Technol. 2005; 11(1):17–26. [PubMed: 15691255]
27. Dalal A, Moss RH, Stanley RJ, Stoecker WV, Gupta K, Calcara DA, et al. Concentric decile segmentation of white and hypopigmented areas in dermoscopy images of skin lesions allows discrimination of malignant melanoma. Comput Med Imaging Graph. 2011; 35(2):148–54. [PubMed: 21074971]
28. Fan RE, Chen PH, Lin CJ. Working set selection using second order information for training SVM. JMLR. 2005; 6:1889–918.
29. Chang, CC.; Lin, CJ. LIBSVM: a library for support vector machines. Software available at http://www.csie.ntu.edu.tw/~cjlin/libsvm [Last visited 14.03.14]
30. Terushkin V, Dusza SW, Mullani NA, Duvic M, Zouridakis G, Weinstock M, et al. Transillumination as a means to differentiate melanocytic lesions based on their vascularity. Arch Dermatol. 2009; 145(9):1060–2. [PubMed: 19770455]
31. Menzies SM, Kreusch J, Byth K, Pizzichetta MA, Marghoob A, Braun R, et al. Dermoscopic evaluation of amelanotic and hypomelanotic melanoma. Arch Dermatol. 2008; 144(9):1120–7. [PubMed: 18794455]

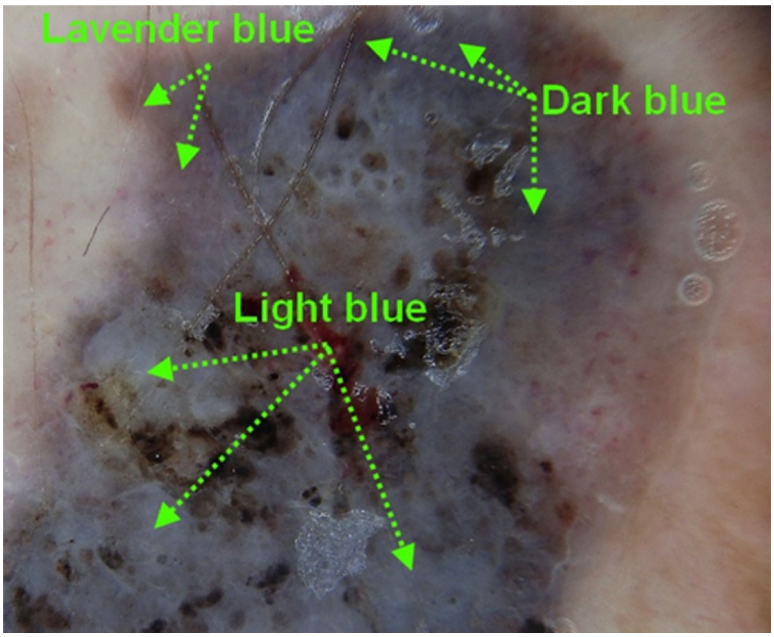

Fig. 1.

Dermoscopy image of invasive melanoma illustrating three shades of blue indicative of pigmented nodular melanoma. (For interpretation of the references to color in this figure legend, the reader is referred to the web version of this article.)

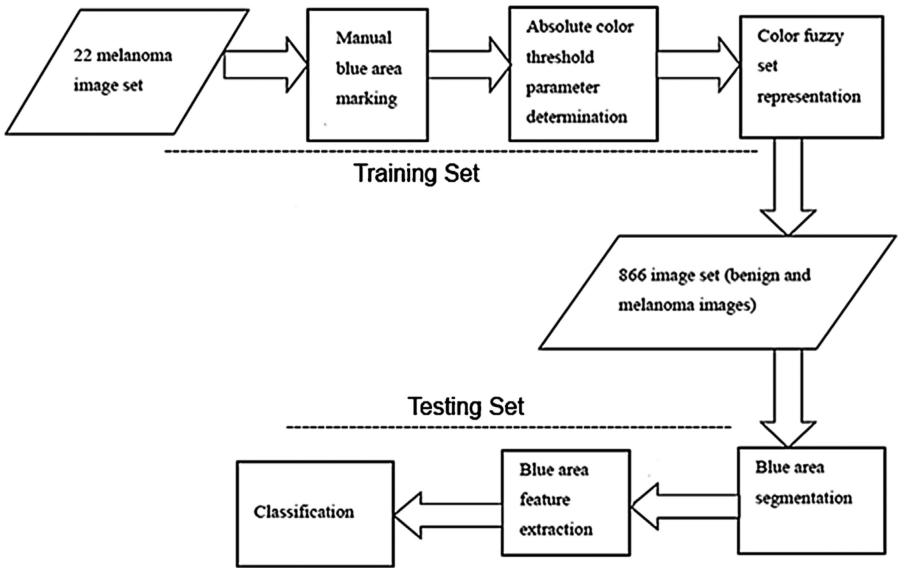

Fig. 2.
Blue area workflow overview.

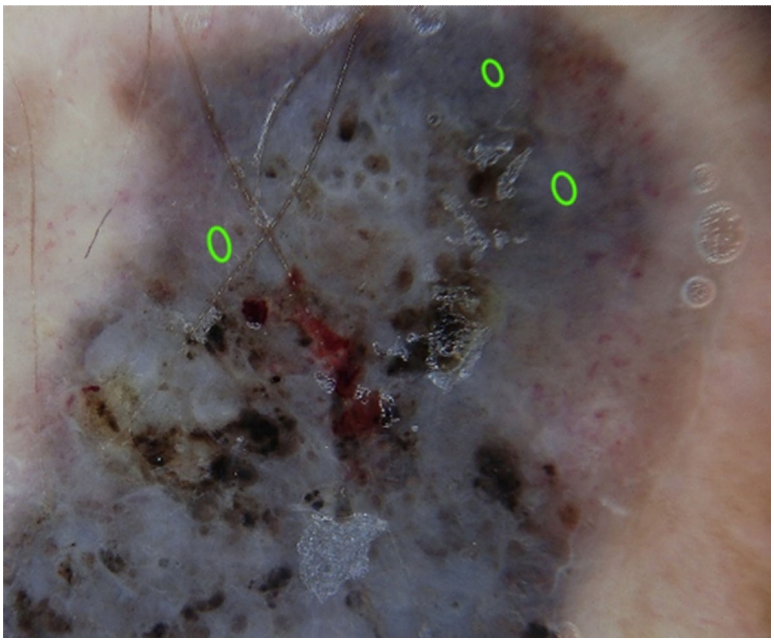

Fig. 3.

Blue areas selected for analysis. (For interpretation of the references to color in this figure legend, the reader is referred to the web version of this article.)

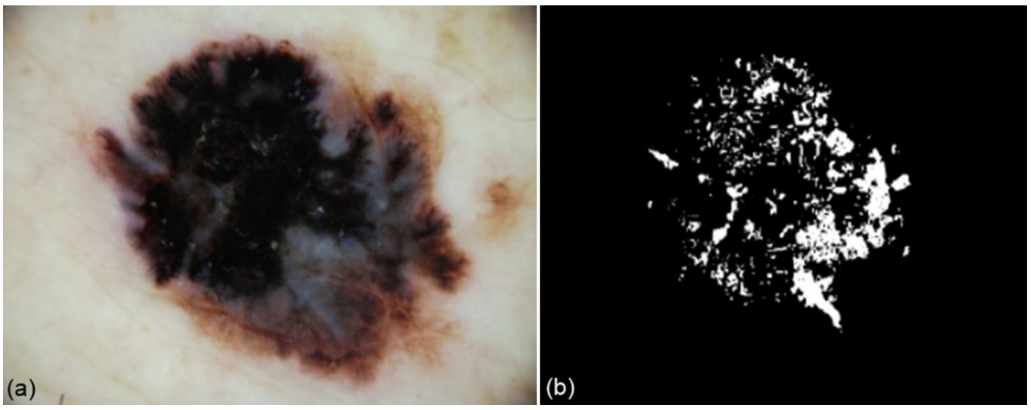

Fig. 4.
(a) Melanoma image. (b) Blue area mask generated from chromaticity thresholds.

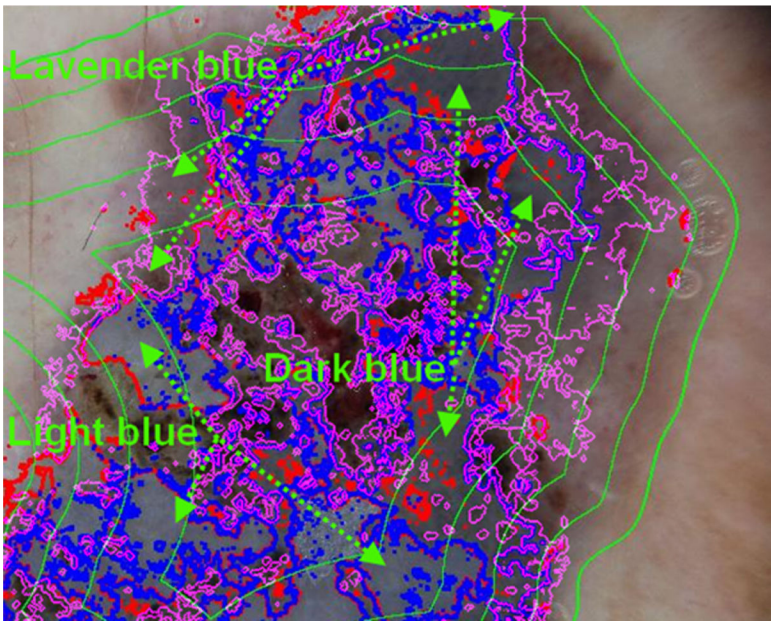

Fig. 5.

Melanoma with three shades of blue, optimized chromaticity and brightness thresholds, with quintile overlays. (For interpretation of the references to color in this figure legend, the reader is referred to the web version of this article.)

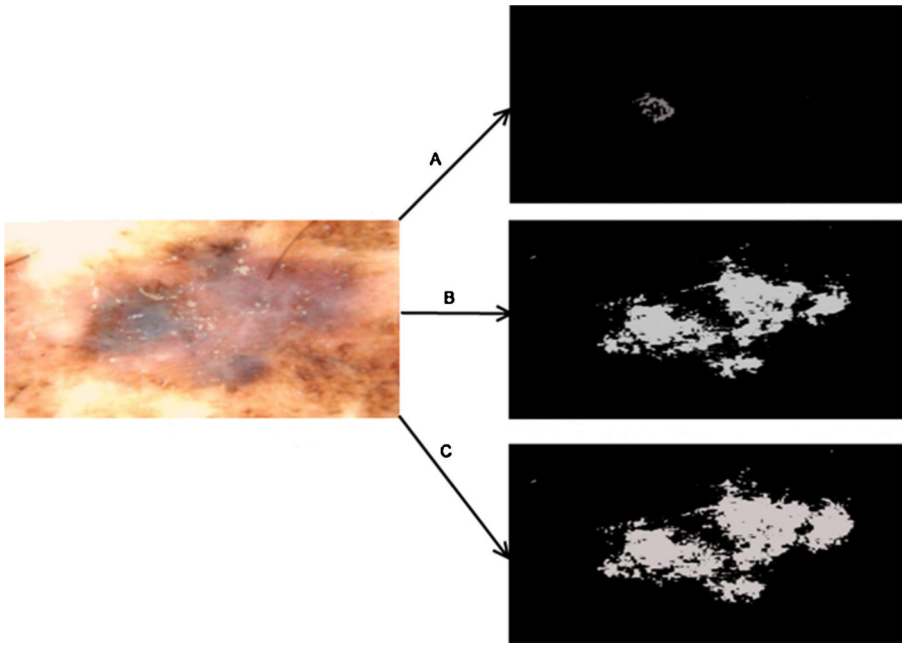

Fig. 6.

Dermoscopy image of melanoma and resultant lavender blue area masks with alpha cuts at (A) 1, (B) 0.5, and (C) 0.25. (For interpretation of the references to color in this figure legend, the reader is referred to the web version of this article.)

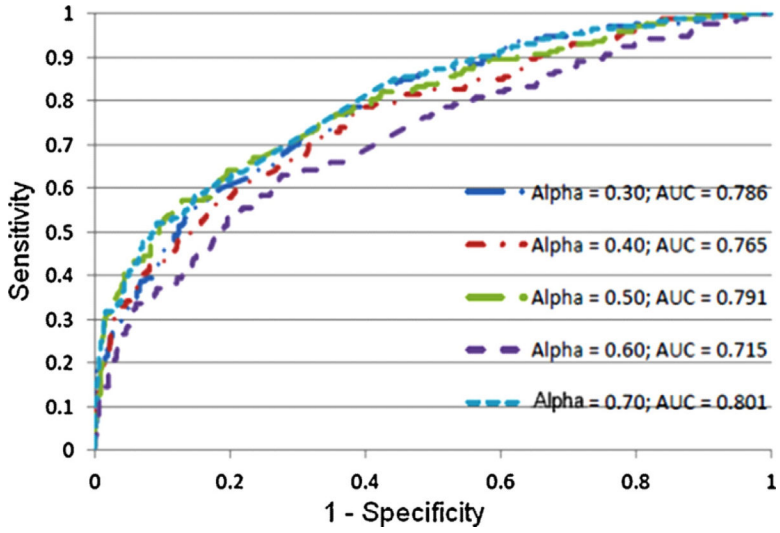

Fig. 7.

Receiver operating characteristic curve from the logistic regression models; AUC = area under the curve.

Table 1

Corner points of membership functions for color parameters to segment blue areas.

	Membership function	*a*	*b*	*c*	*d*
Red chromaticity (light blue)	$\mu_{red\_chrom}(\chi)$	0.21	0.27	0.34	0.4
Red chromaticity (dark blue)	$\mu_{red\_chrom}(\chi)$	0.21	0.27	0.34	0.4
Red chromaticity (lavender blue)	$\mu_{red\_chrom}(\chi)$	0.33	0.34	0.38	0.5
Blue chromaticity (light blue)	$\mu_{blue\_chrom}(\chi)$	0.24	0.3	0.43	0.49
Blue chromaticity (dark blue)	$\mu_{blue\_chrom}(\chi)$	0.24	0.3	0.43	0.49
Blue chromaticity (lavender blue)	$\mu_{blue\_chrom}(\chi)$	0.24	0.32	0.38	0.42
Green chromaticity (lavender blue)	$\mu_{gree\_chrom}(\chi)$	0.32	0.38	–	–
Relative color (light blue)	$\mu_{rel\_color}(\chi)$	0	10	–	–
Relative color (dark blue)	$\mu_{rel\_color}(\chi)$	0	10	–	–
Relative color (lavender blue)	$\mu_{rel\_color}(\chi)$	15	30	–	–

Table 2

Support vector machine results for diagnostic melanoma accuracy based on varied alpha cuts for three shades of blue: Individual shades *vs.* all 3 shades.

Alpha cuts applied to color features	Light blue (%)	Dark blue (%)	Lavender blue (%)	All three shades (%)
0.25	80.1	80.0	80.0	80.74
0.30	80.0	80.0	80.0	81.19
0.35	80.0	80.0	80.0	81.19
0.4	80.0	79.9	80.0	81.42
0.45	79.9	79.9	80.0	81.42
0.5	80.0	79.8	80.0	80.63
0.55	79.9	79.8	80.0	80.96
0.6	80.0	79.8	80.0	80.74
0.65	80.1	79.9	80.0	80.29
0.7	80.1	79.9	80.0	79.95
0.75	80.0	80.0	79.9	79.62
1	79.9	80.1	79.9	79.39

Table 3

Accuracy results based on support vector machine and logistic regression with statistical analysis software (SAS) different alpha cuts for combined shades.

Alpha cuts	Support vector machine (maximum correct) (%)	Logistic regression (maximum correct) (%)	Logistic regression estimated area under the curve (%)
0.25	81.4	82.2	76.9
0.30	81.2	82.7	78.6
0.35	80.7	82.3	75.3
0.40	80.6	82.7	76.5
0.45	80.6	82.3	77.1
0.50	80.4	82.3	79.1
0.55	80.0	82.4	76.1
0.60	79.9	81.4	71.5
0.65	79.8	82.7	78.8
0.70	79.7	81.9	80.1
0.75	79.3	81.9	77.3
1.00	80.3	81.8	68.0

Table 4

Statistical summary for eight significant variables ($p \leq 0.05$) retained (of 150 variables analyzed) in final model, all 3 shades, accuracy maximized at 82.7% for alpha cut = 0.65.

Feature description (all features from sections E and F)	Wald Chi-square	*p*-Value
Green Chromaticity (lavender blue)	14.67	0.0001
Average Blue Color (dark blue)	12.06	0.0005
Eccentricity of Largest Blob (light blue)	2.56	0.0057
Area (dark blue)	1.73	0.05
Average Blue Color (lavender blue)	9.60	0.002
Red Minimum (lavender blue)	4.65	0.03
Blue Chromaticity (lavender blue)	5.42	0.02
Green Smoothness (lavender blue)	9.24	0.001